# Detection of Potential Transit Signals in Sixteen Quarters of Kepler Mission Data

Peter Tenenbaum, Jon M. Jenkins, Shawn Seader, Christopher J. Burke, Jessie L. Christiansen, Jason F. Rowe, Douglas A. Caldwell, Bruce D. Clarke, Jeffrey L. Coughlin, Jie Li, Elisa V. Quintana, Jeffrey C. Smith, Susan E. Thompson, and Joseph D. Twicken

SETI Institute/NASA Ames Research Center, Moffett Field, CA 94305, USA

peter.tenenbaum@nasa.gov

Michael R. Haas, Christopher E. Henze, Roger C. Hunter, and Dwight T. Sanderfer

NASA Ames Research Center, Moffett Field, CA 94305, USA

Jennifer R. Campbell, Forrest R. Girouard, Todd C. Klaus, Sean D. McCauliff, Christopher K. Middour, Anima Sabale, Akm Kamal Uddin, and Bill Wohler

Orbital Sciences Corporation/NASA Ames Research Center, Moffett Field, CA 94305, USA

and

Thomas Barclay and Martin Still

BAER Institute/NASA Ames Research Center, Moffett Field, CA 94305, USA

#### ABSTRACT

We present the results of a search for potential transit signals in four years of photometry data acquired by the *Kepler* Mission. The targets of the search include 111,800 stars which were observed for the entire interval and 85,522 stars which were observed for a subset of the interval. We found that 9,743 targets contained at least one signal consistent with the signature of a transiting or eclipsing object, where the criteria for detection are periodicity of the detected transits, adequate signal-to-noise ratio, and acceptance by a number of tests which reject false positive detections. When targets that had produced a signal were searched repeatedly, an additional 6,542 signals were detected on 3,223 target stars, for a total of 16,285 potential detections. Comparison of the set of detected signals with a set of known and vetted transit events in the *Kepler* field of view shows that the recovery rate for these signals is 96.9%. The ensemble properties of the detected signals are reviewed.

Subject headings: planetary systems – planets and satellites: detection

#### 1. Introduction

We have reported on the results of past searches of the *Kepler* Mission data for signals of transiting planets, in particular the search of the first three quarters (Tenenbaum et al. 2012) and the search of the first three years (Tenenbaum et al. 2013). We now update and extend those results to incorporate an additional year of data acquisition and an additional year of *Kepler* Pipeline development.

#### 1.1. Kepler Science Data

The details of Kepler operation and data acquisition have been reported elsewhere (Haas et al. 2010). In brief: the Kepler spacecraft is in an Earth-trailing heliocentric orbit and maintained a boresight pointing centered on  $\alpha = 19^{\rm h}22^{\rm m}40^{\rm s}, \delta = +44.5^{\circ}$ . The Kepler photometer acquired data on a 115 square degree region of the sky. The data were acquired in 29.4 minute integrations, colloquially known as "long cadence" data. The spacecraft was required to rotate about its boresight axis by 90 degrees every 93 days in order to keep its solar panels and thermal radiator correctly oriented; the interval which corresponds to a particular rotation state is known colloquially as a "quarter." Because of the quarterly rotation, target stars were observed throughout the year in 4 different locations on the focal plane. Science acquisition was interrupted monthly for data downlink, quarterly for maneuver to a new roll orientation (typically this is combined with a monthly downlink to limit the loss of observation time), once every 3 days for reaction wheel desaturation (one long cadence sample is sacrificed at each desaturation), and at irregular intervals due to spacecraft anomalies. In addition to these interruptions which were required for normal operation, data acquisition was suspended for 11.3 days, from 2013-01-17 19:39Z through 2013-01-29 03:50Z (555 long cadence samples) <sup>2</sup>: during this time, the spacecraft reaction wheels were commanded to halt motion in an effort to mitigate damage which was being observed on

 $<sup>^1\</sup>mathrm{Current}$  affiliation: NASA Exoplanet Science Institute, California Institute of Technology, Pasadena, CA 91125, USA

<sup>&</sup>lt;sup>2</sup>Time and date are presented here in ISO-8601 format, YYYY-MM-DD HH:MM, or optionally YYYY-MM-DD HH:MM:SS, with a trailing 'Z' to denote UTC.

Reaction Wheel 4, and spacecraft operation without use of reaction wheels is not compatible with high-precision photometric data acquisition.

In July 2012, one of the four reaction wheels used to maintain spacecraft pointing during science acquisition experienced a catastrophic failure. The mission was able to continue, using the remaining three wheels to permit 3-axis control of the spacecraft, until May of 2013. At that time a second reaction wheel failed, which forced an end to *Kepler* data acquisition in the nominal *Kepler* field of view. As a result, the analysis reported here is the first which incorporates the full volume of data acquired from that field of view.

Kepler science data acquisition began at 2009-05-12 00:00Z, and acquisition of Quarter 16 data concluded at 2013-04-08 11:17:11Z. This time interval contains 69,810 long cadence intervals. Of these, 4,726 were consumed by the interruptions listed above, and 65,084 long cadence intervals were dedicated to science data acquisition. An additional 1,076 long cadence intervals were excluded from use in searches for transiting planets. These samples were excluded due to data anomalies which came to light during processing and inspection of the flight data. This includes a contiguous set of 255 long cadence samples acquired over the 5.2 days which immediately preceded the 11 day downtime described above: the shortness of this dataset combined with the duration of the subsequent gap led to a judgement that the data would not be useful for transiting planet searches.

A total of 197,322 targets observed by Kepler were searched for evidence of transiting planets. This set of targets includes all stellar targets observed by Kepler at any point during the mission, and specifically includes target stars which were not originally observed for purposes of transiting planet searches (asteroseismology targets, guest observer targets, etc.). The exception to this is a subset of known eclipsing binaries, as described below. Figure 1 shows the distribution of targets according to the number of quarters of observation. A total of 111,800 targets were observed for all 16 quarters. An additional 39,964 targets were observed for 13 quarters: the vast majority of these targets were in regions of the sky which are observed in some quarters by CCD Module 3, which experienced a hardware failure in its readout electronics during Quarter 4, resulting in a "blind spot" which rotates along with the Kepler spacecraft. The balance of 45,558 targets which were observed for some other number of quarters is largely due to gradual changes in the target selection process over the duration of the mission.

As described in Tenenbaum et al. (2013), some known eclipsing binaries are excluded from planet searches. In this case, a total of 1,519 known eclipsing binaries were excluded. This number is smaller than the number excluded in the Q1-Q12 analysis due to a change in exclusion criteria. Specifically, we excluded eclipsing binaries from the most recent Kepler catalog of eclipsing binaries (Kirk et al. 2013) that did not meet the criteria of being "transit-

like". Eclipsing binaries were considered to be transit-like only if all of the following criteria were met:

- 1. The primary eclipse depth is greater than or equal to zero, i.e., flux must decrease at primary eclipse
- 2. The primary and secondary eclipse depths are within 10% of each other OR the secondary eclipse depth is less than 10% of the primary eclipse depth
- 3. If detected, the phase of secondary eclipse has to occur within the range 0.49 0.51, i.e., the binary star's orbit must be near-circular
- 4. The morphology of the system, as defined in Kirk et al. (2013), has to be < 0.6, i.e., the primary and secondary eclipses must be well separated from one another.

Thus, the excluded eclipsing binaries are largely contact binaries which produce the most severe misbehavior in the Transiting Planet Search (TPS) pipeline module Tenenbaum et al. (2012, 2013), while well-detached, transit-like eclipsing binaries are now processed in TPS. This was done in order to ensure that no possible transit-like signature was excluded, and also to produce examples of the outcome of processing such targets through both TPS and Data Validation Wu et al. (2010); Twicken et al. (2014), such that quantitative differences between planet and eclipsing binary detections could be determined and exploited for rejecting other, as-yet-unknown, eclipsing binaries detected by TPS.

#### 1.2. Processing Sequence: Pixels to TCEs to KOIs

The steps in processing *Kepler* science data have not changed since Tenenbaum et al. (2012), and are briefly summarized below. The pixel data from the spacecraft were first calibrated to remove pixel-level effects such as gain variations, linearity, and bias. The calibrated pixel values were then combined within each target to produce a flux time series for that target. The ensemble of target flux time series were then corrected for systematic variations driven by effects such as differential velocity aberration, temperature changes, and small instrument pointing excursions. These corrected flux time series became the inputs for the Transiting Planet Search.

The Transiting Planet Search (TPS) software module analyzed each corrected flux time series individually for evidence of periodic reductions in flux which would indicate a possible transiting planet signature. The search process incorporated a significance threshold (often referred to as the "multiple event statistic") and a series of vetoes; the latter were necessary because while the significance threshold was sufficient for rejection of the null hypothesis, it was incapable of discriminating between multiple competing alternate hypotheses which can potentially explain the flux excursions. An ephemeris on a given target which satisfied the significance threshold and passed all vetoes is known as a Threshold Crossing Event (TCE). Each target with a TCE was then searched for additional TCEs, which potentially indicated multiple planets orbiting a single target star.

After the search for TCEs concluded, additional automated tests were performed to assist members of the Science Team in their efforts to reject false positives. A TCE which has been accepted as potential transiting planets, based on analysis of these additional tests, is designated as Kepler Objects of Interest (KOIs). Note that, while the TCEs were determined in a purely algorithmic fashion by the TPS software module, KOIs have been selected on the basis of examination and analysis by human scientists.

# 1.3. Pre-Search Processing

Since the publication of Tenenbaum et al. (2013), there have been considerable improvements to the Pre-Search Data Conditioning (PDC) component of the Kepler pipeline. The purpose of PDC is to remove variations in the flux time series which are generated by changes in the spacecraft environment or other systematic effects. PDC performs very well for the majority of targets in the Kepler Field of View. However, for an appreciable minority the Bayesian Maximum A Posteriori (PDC-MAP) algorithm (Smith et al. 2012) does not produce acceptable corrections of the visible systematics. To further minimize the number of targets for which PDC-MAP fails to perform admirably, a new method has been developed: multi-scale MAP (or msMAP) (M.C. Stumpe et al., 2014, in preparation). Utilizing an overcomplete discrete wavelet transform the new method divides each light curve into multiple channels, or bands, based upon characteristic signal scales in time and frequency. This produces three time series for each flux time series: one dominated by each of short-timescale (< 3 long cadences), medium-timescale (4 to 1023 long cadences), and long-timescale (1024 or more long cadences) variations. The PDC-MAP algorithm is then applied to each band separately, which allows for a better separation of characteristic signals and cleaner removal of the systematics. Relevant to transit detection, the new msMAP provides two distinct improvements to the PDC processed data. The first is a significantly improved removal of thermal transients which occur in the transition from Earth-pointing to science pointing after each data downlink. The second is a modest reduction in introduced noise.

A second significant improvement to PDC is that it now "protects" known transits

from false detection as Sudden Pixel Sensitivity Dropouts (SPSDs) or other types of outlier. Cadences containing known transits and eclipses are computed using the known epoch, period and duration of the events, and assuming a linear ephemeris. No SPSDs or outliers are flagged during the known transits. This helps preserve transit depths and shapes from corruption by the SPSD and outlier correction algorithms. Note that this only affects known transits. There is still the risk of transit corruption for as yet undetected transits. However, once the transits are detected and validated, subsequent data processing iterations will incorporate the new information.

# 2. Transiting Planet Search

This section describes the changes which have been made to the TPS algorithm since Tenenbaum et al. (2013). For further information on the algorithm, see Jenkins (2002), Jenkins et al. (2010b), and Tenenbaum et al. (2012).

#### 2.1. Removal of Positive Flux Outliers

As described in Section 2.4 of Tenenbaum et al. (2013), removal of negative flux outliers is a hazardous action, since it relies upon an algorithmic capability to distinguish between a true outlier and a transit, and for obvious reasons removing the latter is frowned upon. For this reason, strict limitations are placed upon the algorithm's capabilities for removing suspected negative outliers.

Positive outliers are much less risky to remove, since by definition a positive outlier looks like the opposite of a transit. At first glance, one might therefore assume that positive flux outliers are irrelevant as a source of false alarms or other difficulties, since the difference between a short-duration positive flux excursion and a short-duration negative flux excursion is intuitively obvious to the most casual observer. In actuality, however, positive flux excursions can result in false alarm detections via the following mechanism: when a positive flux excursion is subjected to the whitening filter, the whitened result includes ringing which precedes and follows the excursion, as shown in Figure 2. The strongest components of the ring-down have the opposite sign to the original excursion, thus a positive excursion in the flux results in two negative excursions in the whitened flux, which are often misconstrued as transits by the subsequent search.

The removal of positive outliers is accomplished by marking their locations in the quarter-stitched flux time series as gaps and applying the standard TPS gap filling algo-

rithm. The identification of positive outliers, by contrast, makes use of the whitened flux. The advantage to this is that by design the whitened flux contains only Gaussian-distributed, zero mean, unit variance white noise, plus quasi-impulsive outliers; consequently, the positive outliers are extremely easy to identify in the whitened flux. The disadvantage is that a positive outlier in the whitened flux can either indicate a positive outlier in the original flux, or it can be part of the ring-down of a negative outlier such as a transit; this can be visualized by inverting the lower plot in Figure 2. Thus the algorithm for positive outlier removal is as follows:

- whiten the quarter-stitched flux
- identify clusters of whitened flux values which exceed a threshold: in this case a threshold of 12.3  $\sigma$  is used, as explained in Appendix A
- determine whether each cluster is due to positive outliers in the original flux or due to the ring-down of negative outliers in the original flux: this is accomplished by examining the local minima adjacent to each cluster, since for positive outliers the local minima will be weaker than the positive outliers, whereas for the ring-down of a transit one of the local minima will be much stronger than the positive outliers
- for each positive outlier value thus identified, mark the cadences in the quarter-stitched flux as gapped and apply gap-filling
- produce a new whitened flux from the outlier-removed quarter-stitched flux and iterate the process until no further positive outliers are identified: this takes account of the fact that removal of outliers can change the local noise characteristics slightly, causing values which had previously been below threshold to exceed the threshold.

#### 2.2. Limitation on Allowable Transit Duty Cycles

An additional means of separating likely transiting planet signatures from false alarms is to apply bounds to the ratio of the transit duration  $\tau$  to the orbital period T. The relationship between these parameters of the transit can be derived from Kepler's laws of motion:

$$\tau = kT^{1/3}. (1)$$

We can rewrite Equation 1 in terms of the transit duty cycle  $\phi_{\text{dut}} \equiv \tau/T$ :

$$\phi_{\text{dut}} = kT^{-2/3}.\tag{2}$$

The value of k for a specific system is a function of the star's properties, and also the eccentricity of the orbit which is under consideration. For circular orbits about the Sun, k is approximately 0.058 days<sup>2/3</sup> (Gilliland et al. 2000); for a circular orbit about a late-type M dwarf star, k is approximately 0.026 days<sup>2/3</sup>.

The shortest orbital period included in TPS searches is set to 0.5 days. At this limit, Equation 2 shows that  $\phi_{\text{dut}}$  for a Sun-like star and a circular orbit is approximately 0.092. To allow margin for elliptical orbits or stars which are far from Solar in their parameters, we limit the maximum allowed value of  $\phi_{\text{dut}}$  to 0.16. This restriction is implemented by adjusting the minimum search period for each trial transit duration used in the search: for 1.5-hour transits, the search is allowed to operate down to periods of 0.5 days, while for 15-hour transits the minimum search period is limited to 3.9 days. This restriction was also enforced in the Q1-Q12 processing reported in Tenenbaum et al. (2013).

In the Q1-Q16 processing, an additional restriction was placed on the lower bound of allowed  $\phi_{\rm dut}$  values, specifically

$$\phi_{\text{dut}} \ge 0.017T[\text{days}]^{-2/3}.$$
 (3)

This limit is 3.4 times smaller than that expected for Solar stars and 1.5 times smaller than expected for late M dwarf stars, which allows margin for elliptical orbits, large impact parameter values, and non-Solar parameters. Equation 3 sets a maximum search period which is a function of transit duration: for example, 1.5-hour transits are limited to search periods of 50 days or less, while 3.0-hour transits are limited to search periods of 300 days or less.

Note that the use of the duty cycle cuts creates an implicit trade-off between the purity of the search (i.e., rejection of false positives) and its efficiency (i.e., acceptance of true positives). Specifically, the cuts will reject false positive detections around Sun-like stars on the basis of unphysicality. At the same time, the upper limit on permitted duty cycle will reject some true positive detections on stars which are significantly larger than the Sun; the lower limit on permitted duty cycle will reject some true positive detections on stars which are significantly smaller than the Sun; and both cuts can potentially reject true positive detections on Sun-like stars from planets with highly eccentric orbits. It is our judgement that the regions of parameter space excluded by these cuts are acceptably small when both sides of the trade-off are considered.

# 2.3. Detection and Vetoing of Potential Signals

Out of the 197,322 targets which were searched by TPS, a total of 112,981 were found to have at least one periodic signal which exceeded the multiple event statistic of 7.1  $\sigma$ , while 84,341 had no such signal. In this regard, current experience is consistent with past TPS analyses, in which the number of targets for which the maximum multiple event statistic exceeded the detection threshold was unphysically large, implying that the vast majority of these events are false alarms. As in the past, a series of vetoes are used to eliminate false alarms to the extent possible without rejecting excessive numbers of true transit signals. The vetoes which are used in the current analysis – a robust statistic and a series of vetoes based upon  $\chi^2$  statistics – are described in modest detail in Tenenbaum et al. (2013), and in particular the  $\chi^2$  vetoes are described in considerable detail in Seader et al. (2013), so only a description of changes to these quantities will be given here.

The multiple event statistic as well as the robust statistic only admit detections with three or more transits. In detections where there are only three transits, the multiple event statistic is blind to the quality of each transit whereas the robust statistic scrutinizes each of the three transits to veto situations where one or more of the three transits overlaps significantly with a region of data that is anomalous in some way. The algorithm for examining the transits for this case has changed slightly from that employed to produce the Q1-Q12 results in Tenenbaum et al. (2013). The past algorithm required that no more than 50% of in-transit cadences be marked as anomalous for any of the three transits, whereas the current algorithm requires that the average of the in-transit data quality weights be at least 0.5. Making this slight change has exposed an undesired sensitivity in the robust statistic algorithm. This change is responsible for an increase in long period false alarms which is discussed in Section 3. Future development work will be directed at enabling the  $\chi^2$  vetoes to identify these long period false alarms by including the data quality weights in the calculation of the degrees of freedom of the statistic (which are ultimately used in the computation of the reduced  $\chi^2$ ).

The two versions of the  $\chi^2$  vetoes described in Tenenbaum et al. (2013) are again employed to produce the results of this paper. The first of these,  $\chi^2_{(1)}$ , remains unchanged. There are some subtle issues, however, associated with the construction of  $\chi^2_{(2)}$  which are discussed at length in Seader et al. (2013) but will be briefly mentioned here for completeness. Correcting for these subtleties enhances the vetoing efficiency of  $\chi^2_{(2)}$  by enabling both the quantities it is computed from and the statistic itself to have the correct statistical properties as described in both Allen (2004) and Seader et al. (2013). The first subtlety is that the  $\chi^2_{(2)}$  calculation implicitly requires that the calculated noise properties of the flux time series are not changed by the presence or absence of a transit signal. In fact, while the noise

calculation is relatively robust against the effect of transits, it is not formally invulnerable: while the presence or absence of a transit results in a change in the noise estimate which is small enough to be neglected in the Multiple Event Statistic calculation, it was found to have an effect on the value of  $\chi^2_{(2)}$ . This is addressed by applying the TPS auto-regressive gap-fill algorithm to the cadences which are in-transit, which produces a flux time series which is effectively transit-free; this time series is used to calculate the noise properties of the flux time series for the purpose of  $\chi^2$  discriminator calculations. The remaining subtleties arise from the assumption that each transit is localized in time and isolated from every other transit (i.e., the transit model consists of a series of short intervals of negative values separated by longer intervals of zero values). While this is true for the unwhitened transit model, it is not true for the whitened transit model, which is the model which must be used in the calculation of the discriminators: in the whitened domain, the transits are "smeared," such that there are no cadences which have a model value of zero, and thus the value of the model at one transit depends to greater or lesser extent on the values of all the other transits. To mitigate the effects, the  $\chi^2$  contribution from each transit is calculated with all other transits replaced by the auto-regressive gap fill values used for the noise calculation, thus effectively performing the calculation for each transit as though it was the only transit in the flux time series; in addition, the calculation neglects any cadence which is outside of that transit, as determined by the unwhitened model, so that the effect of "smearing" into out-of-transit cadence times is eliminated.

In addition to the above changes to existing vetoes, another version of the  $\chi^2$  veto was implemented that is more akin to a classical  $\chi^2$  and is described in great detail in Seader et al. (2013) as  $\chi^2_{(3)}$ . In this version, each single event statistic is compared with a calculated expectation value in the whitened time domain (to avoid the subleties mentioned above). These differences are then summed according to the exact expression for a classical  $\chi^2$ , including division by the expectation value. The thresholding on this statistic is done in the same manner as the previous two  $\chi^2$  statistics as described in both Tenenbaum et al. (2013) and Seader et al. (2013). It was discovered through the course of analysis of these results that  $\chi^2_{(3)}$  works well to veto short period false alarms but the threshold used was too aggressive and is largely responsible for the cases of known short-period transits which were not detected in the most recent processing. Work is currently underway to tune all the vetoes more appropriately.

As mentioned above, the number of targets with a multiple event statistic above the detection threshold was 112,981. The vetoes were then applied to this set of targets. The robust statistic, with a threshold of  $6.4\sigma$ , vetoed 64,233 target stars, leaving 48,748 targets for which there was at least one signal which passed both the robust statistic and multiple statistic criteria. The final layer of vetoes based on  $\chi^2$  statistics, all with thresholds of  $7.0\sigma$ ,

removed 38,977 targets from consideration, leaving 9,771 target stars which produced at least one threshold crossing event (TCE).

# 2.4. Detection of Multiple Planet Systems

For the 9,771 target stars which were found to contain a threshold crossing event, additional TPS searches were used to identify target stars which host multiple planets. The process is described in Wu et al. (2010) and in Tenenbaum et al. (2013). The multiple planet search incorporates a configurable upper limit on the number of TCEs per target, which is currently set to 10. This limit is incorporated for two reasons. First, limitations on available computing resources translate to limits on the number of searches which can be accommodated, and also on the number of post-TPS tests which can be accommodated. Second, applying a limit to the number of TCEs per target prevents a failure mode in which a flux time series is so pathological that the search process becomes "stuck," returning an effectively infinite number of nominally-independent detections which all have the same ephemeris. The selected limit of 10 TCEs is based on experience: to date, the maximum number of KOIs on a single target star is 7, which indicates that at this time limiting the process to 10 TCEs per target is not sacrificing any potential KOIs.

The additional searches performed for detection of multiple planet systems yielded 6,573 additional TCEs across 3,229 target stars, for a grand total of 16,344 TCEs. Note that all of these TCEs are subjected to the full TPS process of detection and vetoing described above.

In the analyses below, a small number of the 16,344 TCEs are not included. This is due to the desire to limit the analysis presented here to TCEs for which there is a full analysis available from the Data Validation (DV) pipeline module (Wu et al. 2010). A total of 28 targets, containing 55 TCEs, failed to complete their DV analyses and are thus excluded. A total of 4 targets produced 11 TCEs each, in excess of the 10 planet limit set as a user-specified parameter for DV; in these cases, the eleventh TCE was reported but not included in the subsequent DV analysis. Considering these exclusions, a total of 9,743 targets produced 16,285 TCEs which are analyzed below. Only the 16,285 TCEs included in this analysis will be exported to the tables maintained by the NASA Exoplanet Archive<sup>3</sup>.

<sup>&</sup>lt;sup>3</sup>http://exoplanetarchive.ipac.caltech.edu.

# 3. Detected Signals of Potential Transiting Planets

As described above, a total of 9,743 targets in the *Kepler* dataset produced TCEs. For 6,520 of these targets, only one TCE was detected; for 3,223 targets, the multiple planet search detected additional TCEs. The total number of TCEs detected across all targets was 16,285. Figure 3 shows the period and epoch of each of the 16,285 TCEs, with period in days and epoch in Kepler-Modified Julian Date (KJD), which is Julian Date - 2454833.0, the latter offset corresponding to January 1, 2009, which was the year of Kepler's launch. Figure 3 also shows the same plot for the 18,427 TCEs detected in the 12 quarter Kepler dataset, as reported in Tenenbaum et al. (2013). The axis scaling is identical for the two subplots, as is the marker size. Several features are apparent in this comparison. First, the number of TCEs is reduced despite the fact that the number of targets and number of quarters of data have both increased since the earlier report, which demonstrates the improved false alarm vetoing logic in the more recent analysis. Second, as expected, the addition of 376 days of data acquisition has increased the parameter space available for detections, as shown by the upward and rightward expansion of the "wedge" in Figure 3 from the Q1-Q12 to the Q1-Q16 results. Third, the distribution of TCE periods appears to be more uniform for long periods in the current analysis, while in the previous one the number of TCEs decreased visibly at longer periods.

The drastic change in the distribution of TCE periods can be seen more clearly in Figure 4, which shows the distribution of TCE periods on a logarithmic scale, with the Q1-Q12 results shown in the upper panel of the figure and the Q1-Q16 results in the middle panel. The more recent search sharply reduces the number of short-period detections, which had dominated the Q1-Q12 processing, but is in turn dominated by long-period detections. The increase in the number of long-period detections in Q1-Q16 compared to Q1-Q12 is vastly larger than would be expected from the addition of 4 quarters of data, and appears to be due entirely to detections which contain 3 valid transits (i.e., there has been no corresponding increase in the number of detections with 4, 5, 6, etc. transits, which would be expected if the new detections were all real events which were made detectable by the additional data). Since the 3 transit events were the only ones affected by the change in the robust statistic described in Section 2.3, our strong suspicion is that the large number of long-period detections is dominated by false alarms which were inadvertently permitted to slip through the system by the aforementioned change.

Figure 5 shows the multiple event statistic (MES) and period of the 16,285 TCEs. The cluster of events with periods above 200 days, with relatively low multiple event statistic, are believed to be another representation of the long-period false alarms discussed above. The relatively narrow cluster at approximately 380 days is due to the "one *Kepler* year" in-

strument artifact discussed in Tenenbaum et al. (2013); this cluster is also visible in Figure 4. Figure 6 shows the distribution of multiple event statistics: 14,506 TCEs with multiple event statistic below 100  $\sigma$  are represented in the left figure, while the right hand figure shows the 10,651 TCEs with multiple event statistic below 20  $\sigma$ . Figure 7 shows the transit duty cycles of the TCEs, with the vertical axis plotted on a logarithmic scale. The strong overabundance of TCEs with extremely low duty cycles is a consequence of the strong overabundance of TCEs with extremely long periods, as discussed above; by contrast with the Q1-Q12 TCEs reported in Tenenbaum et al. (2013), the distribution is relatively flat from transit duty cycles of 0.04 to 0.16.

#### 3.1. Suppression of Long Period False Alarm Detections

While the large number of likely false alarms at long period are not a problem in principle, in practice they represent a complication for the human-labor-intensive process of developing and classifying new *Kepler* Objects of Interest (KOIs) (Batalha et al. 2013). Careful analysis of the statistical properties of the TCEs, and in particular examination of the properties of re-detected known planet candidates and comparison with the ensemble of new TCEs, has allowed the development of a series of "back end" discriminators which reject long-period TCEs that are likely to be false alarms, while preserving long-period TCEs that are more likely to be astrophysical phenomena.

The first discriminator is the ratio of the multiple event statistic (MES) of a given TCE with the variance of the ensemble of MES values on the same target, at the TCE period, but across all phases (MES\_MAD, so named because a median absolute deviation is used to obtain a robust estimate of the variance). In the absence of any transits, the latter ensemble has an expected mean value of zero and unit variance; the presence of transits and/or other low-duty-cycle phenomena results in a long, flat tail to the MES distribution; the presence of more widespread systematic noise in the flux time series will increase the variance of the MES ensemble. Thus, rejecting cases in which the ratio of MES to MES\_MAD is low will remove cases in which the flux time series noise properties are such that the TCE is suspect.

The second discriminator is a comparison of the MES and the signal-to-noise ratio (SNR) of the transit fit performed in Data Validation. The latter is expected to be higher than the former: the Data Validation fit uses a properly-shaped limb-darkened transit model, including fine adjustment of the transit duration, epoch, and period; the MES in the TCE is effectively the SNR achieved by fitting a much lower-fidelity, box-shaped model to the same data. When the ratio of the DV fit SNR to the TCE MES is low, it indicates an event which does not have a transit-like shape. Note that, for some TCEs, no SNR value was available

due to issues in the Data Validation processing. In these cases, the cut on the SNR-to-MES ratio was not applied.

Finally, the MES of the TCE can be compared to the minimum MES on the same target at the TCE period but across all epochs. In the absence of astrophysical signatures, the MES follows a normal distribution with zero mean and unit variance; consequently, the minimum multiple event statistic at the TCE period should be a negative value, and should have a probability distribution given by the negative-valued portion of a Gaussian. The ratio of the absolute value of the minimum multiple event statistic (henceforth MES\_MIN) to the MES of the TCE should therefore be small for a high-quality detection. The presence of periodic positive excursions in the target flux time series at the TCE period indicate a strong probability that some phenomenon other than transits is responsible for the TCE.

After analysis of the properties of the discriminators above, we found that it was possible to remove a significant fraction of the long-period false alarms while preserving the high-quality TCEs. This is accomplished by rejecting a TCE for which any of the following is true:

- 1. MES / MES\_MAD < 7.1,
- 2. SNR / MES < 0.6 (for TCEs which have an SNR value available),
- 3. MES\_MIN / MES > 0.6.

When these cuts were applied to the Q1-Q12 population of planet candidates, it was determined that approximately 1% would be rejected and approximately 99% retained. Applying these cuts to the Q1-Q16 TCEs reduces the number of TCEs to be vetted from 16,285 to 7,959, and of particular importance in this run, from 6,073 to 1,243 with periods of 300 days or more. The bottom panel in Figure 4 shows the distribution of periods for the 7,959 TCEs which passed the cuts listed above.

# 3.2. Comparison with Known Kepler Objects of Interest (KOIs)

As in past analyses (Tenenbaum et al. 2012, 2013), we have identified a subset of the Kepler Objects of Interest (KOIs) which we use as a set of test subjects for the TPS run. TPS does not receive any prior knowledge about detections on targets; therefore, the redetection of objects of interest which were previously detected and classified as valid planet candidates is a valuable test to guard against inadvertent introduction of significant flaws into the detection algorithm.

The list of Q1-Q12 KOIs has been analyzed and a set of high-quality "golden KOIs" identified for comparison to the Q1-Q16 TCEs. This subset of the full KOI list is a representative cross-section of all KOIs in the parameters of transit depth, signal-to-noise, and period, and includes cases which have been identified as eclipsing binaries or astrophysical false positives.

The "golden KOI" set includes 1,646 KOIs across 1,417 target stars. Figure 8 shows the distribution of estimated transit depth, signal-to-noise ratio, and period for the "golden KOIs." Out of these, 1,372 target stars produced one or more TCE, while 45 target stars did not. All 45 of the target stars which produced no TCE have one and only one KOI per target, and the missed KOIs are strongly dominated by short periods: 39 out of 45 have periods under 3 days, and only 1 out of 45 has a period in excess of 1 quarter. Examination of the short period failures indicates that they are dominated by a common failure mode, in which short period transits are mistaken for narrow-band oscillations of the host star and eliminated by an algorithm which is designed to address such narrow-band oscillations (this algorithm is discussed briefly in Section 2 of Tenenbaum et al. (2012)). Note that the oscillations are only removed in instances in which they are strong, i.e., instances in which a small number of narrow-band resonances dominate the stellar variability relative to more broad-band variations. As a consequence, the removed transiting planet signatures have short periods and are strong relative to the background stellar variability. This implies that the resonance removal is primarily a problem for re-detection of planet candidate signatures which were detected early in the Kepler Mission, and has little relevance for detection of weak signals with short periods.

#### 3.2.1. Matching of KOI and TCE Ephemerides

Detection of a TCE on a "golden KOI" target star is a necessary but not sufficient condition to conclude that TPS is functioning properly. An additional step is that the TCEs must be consistent with the expected signatures of the KOIs. This is assessed by comparing the ephemerides of the KOIs and their TCEs, as described in Tenenbaum et al. (2013); the ephemeris-matching process also implicitly compares the numbers of KOIs and TCEs on each target star, which exposes cases in which, on a given star, some but not all KOIs were detected.

Of the 1,601 KOIs on the 1,372 target stars which produced TCEs, it was possible to find matches for 1,597 of the KOIs. The two KOIs which did not produce TCEs were KOI 1101.01 (KIC 3245969), and KOI 351.04 (KIC 11442793). KOI 1101.01 is a short-period candidate (2.84 days), and was most likely removed by the narrow-band oscillation algorithm;

the second candidate on this target, with a period of 11.4 days, was detected with a correct ephemeris match. KOI 351 is a multi-planet system with significant transit timing variations (TTVs) (Cabrera et al. 2014); since TPS requires highly periodic signals to produce a valid detection, its performance on this system has always been poor. Nonetheless, TPS did detect KOI 351.03, KOI 351.05, and KOI 351.06 with correct ephemeris matches, though in the case of 351.05 the match is only approximate (match criterion value of 0.82, indicating overlap between 82% of the transits in the KOI and the TCE).

Figure 9 shows the value of the ephemeris match criterion for the 1,597 KOI-TCE matches, sorted into descending order. A total of 1,569 KOI-TCE matches have a criterion value of 1.0, indicating that each transit predicted by one ephemeris corresponds to a transit predicted by the other, to within one transit duration. In these cases, it has been assumed that TPS correctly detected the "golden KOI" in question and no further analysis was performed.

In the 28 cases in which the ephemeris match was imperfect, each KOI-TCE match was manually inspected. The disposition of the results is as follows:

- In 11 cases, the TCE actually matches the KOI, but the value of the match parameter does not reflect this; in general this is because the KOI ephemeris was derived with early flight data, requiring extrapolation to determine the transit times late in the mission and permitting an accumulation of error in the KOI transit timings relative to the actual timings
- In 13 cases, TPS detected a harmonic or sub-harmonic of the KOI, with a KOI period twice the TCE period the most common by far
- In 2 cases, TPS detected the planet but produced an incorrect ephemeris due to transit timing variations (TTVs)
- In 2 cases, TPS failed to detect the KOI and the TCE appears to be a false alarm.

In conclusion, out of the 28 KOI-TCE pairs which have imperfect ephemeris matches, only 2 actually constitute a failure of the detection algorithm.

In addition to the TCEs described above, there were 476 TCEs detected on the KOI targets which are not on the list of "golden KOIs." The majority of these are known KOIs which were not included on the "golden KOI" list (i.e., cases in which some of the KOIs on a given target star were included while others fell below the threshold for inclusion); in other cases, the unmatched TCE is a secondary eclipse of an eclipsing binary or an occultation of

a large planet behind its host star. In a few cases, these may constitute new detections of additional planet candidates on stars already known to host one or more such candidates.

# 3.2.2. Conclusion of TCE-KOI Comparison

Out of 1,646 "golden KOIs" used to demonstrate the validity of the TPS algorithm, 1595 were correctly detected, for a recovery rate of 96.9%. The missed KOIs were largely overlooked by TPS due to an algorithm which, in removing from the data narrow-band resonances due to stellar variation, occasionally removes short-period transiting planet signatures. This removal issue is not expected to impact future discoveries of transit signatures which are weak relative to the overall stellar variability of their host stars.

#### 4. Conclusions

The Transiting Planet Search (TPS) pipeline module was used to search photometry data for 197,320 Kepler targets acquired over 4 years of science operations. This resulted in the detection of 16,285 threshold crossing events (TCEs) on 9,743 target stars. The distribution of TCEs was qualitatively different from those obtained in a similar search utilizing 3 years of data: the more recent analysis contains a larger proportion of long-period detections which are considered likely false alarms, but a smaller proportion of short-period false alarms. The differences are believed to be due to changes made to the TPS algorithm, rather than to the additional flight data or changes in the data pre-processing algorithms. Out of 1,646 Kepler Objects of Interest (KOIs) used to test the detection and veto algorithms, 1,595 were correctly detected; the missed detections were dominated by short-period objects, and a known limitation of TPS is suspected in these cases.

#### 5. Acknowledgements

Funding for this mission is provided by NASA's Space Mission Directorate. The contributions of Hema Chandrasekaran continue to be essential in the studies documented here.

# A. Determining the Threshold for Positive Outlier Removal

In Section 2.1, an algorithm is described which removes positive outliers from each flux time series prior to searching same for transits. The algorithm requires a threshold for removal of the outliers, which is set at 12.3  $\sigma$ . The rationale behind this value is explained below.

The most obvious requirement for the positive outlier threshold is that it should, indeed, address only outliers and not flux values which are merely above the mean value due to statistical fluctuations. For a whitened flux time series with 69,810 samples, in the limit of Gaussian statistics, we expect that, on average, 1 sample will lie 4.2  $\sigma$  above the mean. Therefore, any threshold which is significantly higher than 4.2  $\sigma$  can be expected to be harmless in terms of its effect on sample values which are driven by statistical fluctuations alone.

Another consideration is that the purpose of removing positive outliers is actually to suppress the formation of transit-like features in the ring-down of the outliers, since the latter can lead to false alarm detections. Given a detection threshold of 7.1  $\sigma$  and a requirement of at least 3 transits for detection, a negative feature with a significance of  $7.1\sigma \times \sqrt{3} = 12.3\sigma$  can exceed the detection threshold when paired with two "transits" which each have a significance of zero. This implies that a transit-like feature with a significance of 12.3  $\sigma$  has a strong probability of triggering a false alarm, and thus our threshold for removing positive outliers should be set such that any outlier which is likely to have a 12.3  $\sigma$  transit-like feature in its ring-down is removed.

Since the ring-down of a positive outlier will always be smaller than the outlier itself, it follows that removing positive outliers with 12.3  $\sigma$  significance is more than sufficient to prevent formation of negative ring-down features with 12.3  $\sigma$  significance. Since 12.3  $\sigma$  is much larger than 4.2  $\sigma$ , it also follows that this threshold will be benign from the point of view of ignoring statistical fluctuations. Thus a threshold of 12.3  $\sigma$  was adopted for positive outlier removal.

#### REFERENCES

Allen, B. 2004, Phys. Rev. D 71, 062001

Batalha, N.M., et al. 2013, ApJS, 204, 24

Borucki, W.J., et al. 2010, ApJ, 713, L126

Cabrera, J., et al. 2014, ApJ, 781, 18

Caldwell, D.A. et al. 2012, ApJ713, L92

Christiansen, J.L. et al. 2012, PASP, 124, 1279

Gilliland, R. L., Brown, T. M., Guhathakurta, P., et al. 2000, ApJ, 545, L47

Gilliland, R.L. et al. 2011, ApJS197, 6

Haas, M.R. et al. 2010, arXiv:1001.0437

Jenkins, J. M. 2002, ApJ, 575, 493

Jenkins, J.M. et al. 2010, arXiv:1001.0258

Jenkins, J.M., et al. 2010, Proc SPIE 7740,77400D

Kirk, B. et al. 2013, in preparation.

Seader, S., et al. 2013, ApJS, 206, 25

Smith, J.C. et al. 2012, PASP124, 1000

Tenenbaum, P. et al. 2012, ApJS199, 24

Tenenbaum, P. et al. 2013, ApJS 206, 5

Twicken, J.D., et al. 2010b, Proc SPIE 7740, 77401U

Twicken, J.D. et al. 2014, in preparation.

Wu, H. et al. 2010, Proc SPIE 7740, 774019

This preprint was prepared with the AAS LATEX macros v5.2.

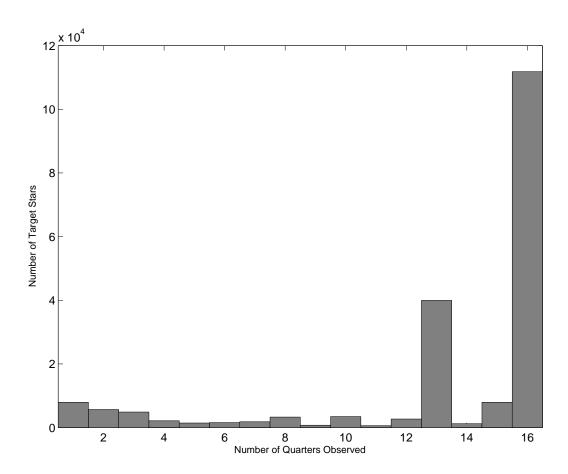


Fig. 1.— Histogram of number of quarters of observation for all targets.

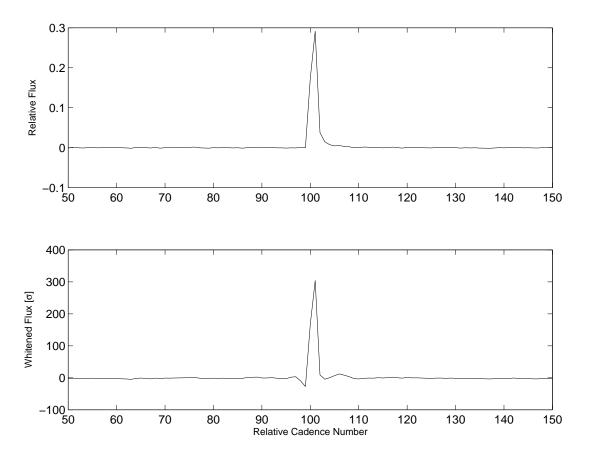


Fig. 2.— Effect of a positive flux outlier. Top: original flux. Bottom: whitened flux. Note that whitening introduces a negative outlier to the whitened flux, which can be misconstrued as a transit. While the resulting negative outlier is much smaller than the original positive outlier, in this case the negative outlier still has a single event significance of over  $27 \sigma$ .

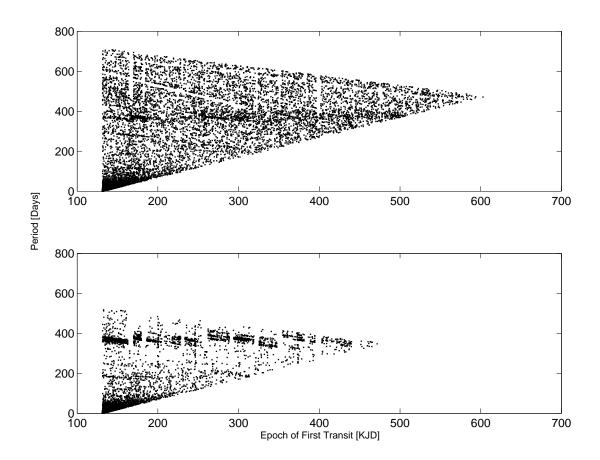


Fig. 3.— Top: epoch and period of the 16,285 TCEs detected in Q1-Q16 of *Kepler* data; bottom: epoch and period of the 18,427 TCEs detected in Q1-Q12 of *Kepler* data, as reported in Tenenbaum et al. (2013). Periods are in days, epochs are in Kepler-modified Julian Date (KJD), see text for definition.

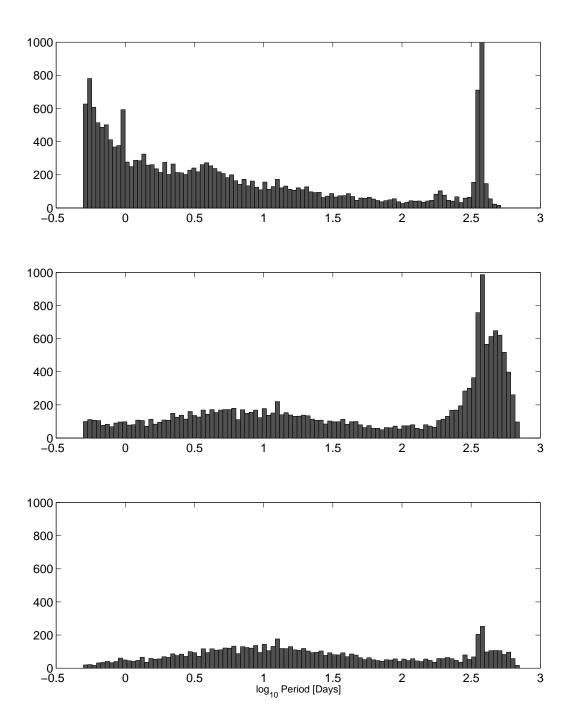


Fig. 4.— Distribution of TCE periods, plotted logarithmically. Top: 18,427 TCEs in the Q1-Q12 search. Middle: 16,285 TCEs in the Q1-Q16 search. Bottom: 7,959 TCEs in the Q1-Q16 search which also pass the additional criteria described in Section 3.1.

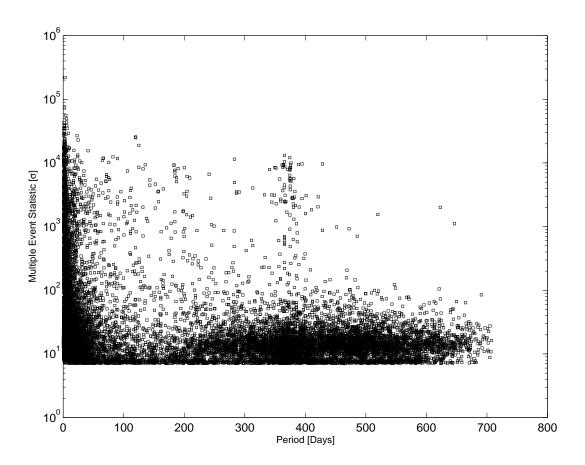


Fig. 5.— Multiple event statistic and orbital period of 16,285 TCEs.

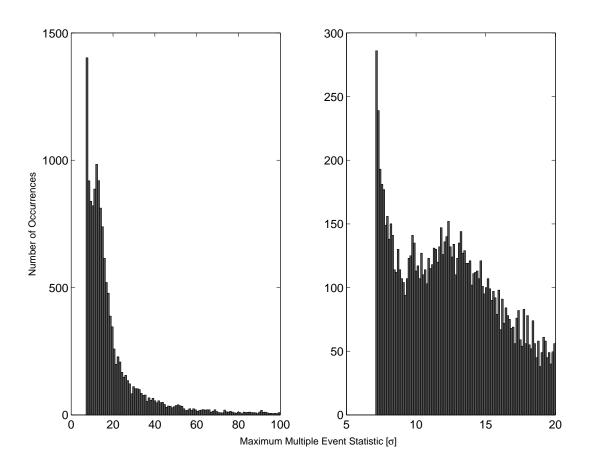


Fig. 6.— Distribution of multiple event statistics. Left: 14,506 TCEs with multiple event statistic below 100  $\sigma$ . Right: 10,651 TCEs with multiple event statistic below 20  $\sigma$ .

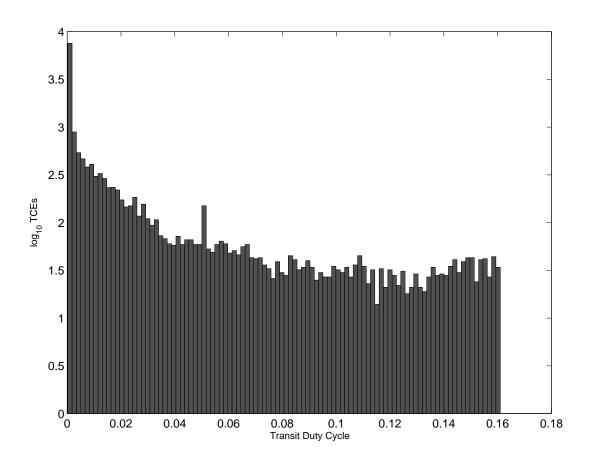


Fig. 7.— Transit duty cycles of TCEs.

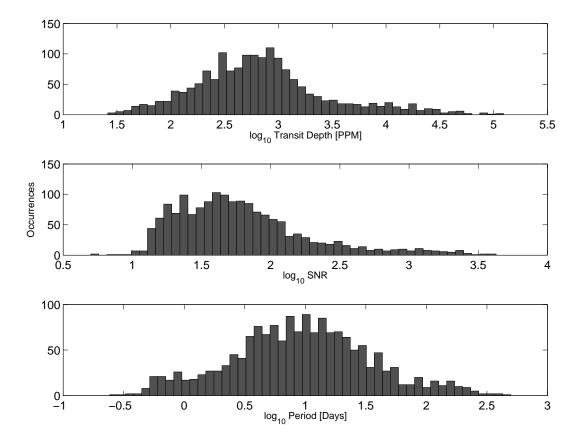


Fig. 8.— Parameter distribution of "golden KOIs." Note use of logarithmic horizontal axes in all cases.

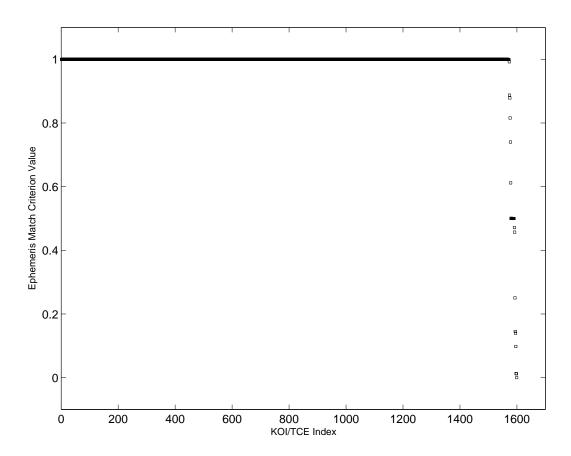


Fig. 9.— Ephemeris match value for 1,599 KOI-TCE matches, sorted into descending order.